

Modeling of rain-wind induced vibrations

Udo Peil[†] and Niklas Nahrath[‡]

Graduate College "Interaction of Structure and Fluid"
Institute for Steel Structures, Technical University of Braunschweig, Germany

(Received January 15, 2002, Accepted November 18, 2002)

Abstract. Rain-wind induced vibrations of cables are a challenging problem in the design of cable-stayed bridges. The precise excitation mechanism of the complex interaction between structure, wind and rain is still unknown. A theoretical model that is able to accurately simulate the observed phenomena is not available. This paper presents a mathematical model describing rain-wind induced vibrations as movement-induced vibrations using the quasi-steady strip theory. Both, the vibrations of the cable and the movement of the water rivulet on the cable surface can be described by the model including all geometrical and physical nonlinearities. The analysis using the stability and bifurcation theory shows that the model is capable of simulating the basic phenomena of the vibrations, such as dependence of wind velocity and cable damping. The results agree well with field data and wind tunnel tests. An extensive experimental study is currently performed to calibrate the parameters of the model.

Key words: rain-wind induced vibration; cable-stayed bridges; guyed mast; cable vibrations; nonlinear dynamics; stability and bifurcation theory

1. Introduction

In the last decade strong cable vibrations have been observed at cable-stayed bridges (Hikami & Shiraishi 1988, Main & Jones 1999, *et al.*). In Germany hangers of an arch bridge showed cracks caused by rain-wind induced vibrations only a few months after erection (Lüesse 1996). The severe low-frequency vibrations only occur in conjunction with the simultaneous action of wind and rain. The fundamental mechanisms have been studied in several field measurements and wind tunnel tests (Verwiebe 1997, Matsumoto 1998 *et al.*). Several researchers have examined the influence of control parameters such as the wind and cable properties or the intensity of rain, but the existing models fail to describe the physics of the problem accurately. In this paper a model is presented that is able to explain the growth mechanism of the vibrations, including the behaviour of the upper rivulet.

In field observations and wind tunnel tests several typical phenomena of rain-wind induced vibrations of low damped, inclined cables have been studied. The vibrations occur only if it rains, whereas the rain intensity is of less importance to excitation. Oscillations have been monitored for drizzle as well as faint to heavy rain. The vibrations occur only in a limited but wide range of relatively low wind velocities. The cables oscillate in one of their first three eigenmodes with amplitudes that can reach a multiple of the cable diameter. The largest vibrations has been observed

[†] Professor, Dr.-Ing.

[‡] Dipl.-Ing. Master of Science

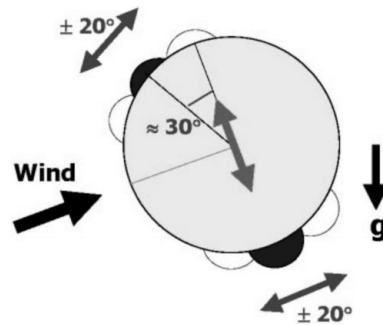


Fig. 1 Rivulets

to occur in cross-wind direction. The vibrations are reduced, if cable damping is increased, e.g. by external dampers.

Possible excitation mechanisms of the rain-wind induced vibrations have been investigated by in-situ measurements and by wind tunnels tests. The restriction of the vibrations to a limited velocity range suggests resonance phenomena like vortex shedding. But the large amplitude and the independence of the eigenfrequencies are more characteristic of movement-induced vibrations like galloping or flutter. Vibrations induced by gusts or parametric excitation are insignificant for this problem.

The growth mechanism of the vibrations is closely linked to the development of water rivulets on the cable surface. The rain moistens the cable surface and the rain water flows down the cable in rivulets. One rivulet forms by gravity on the bottom side of the cable. This lower rivulet is slightly moved leeward by the wind force. Besides the lower rivulet, a second rivulet at the top of the cable has been observed in connection with large cross-wind vibrations. This upper rivulet is mainly held in position by wind forces. It is pitched in a small angle to the wind (Bosdogianni & Olivari 1996). Both rivulets oscillate at the frequency of the cable vibration with an amplitude up to $\pm 20^\circ$. The movements of the rivulets lead to an alteration of the flow cross section. This change in cross section of the body in cross-flow alters the fluid forces in such a way that energy is transferred from the fluid into the structure and the cable starts to oscillate.

Several models to simulate this type of vibration were proposed (Yamaguchi 1990, Geurts & van Staaldunin 1999, Ruscheweyh 1999 *et al.*). Matsumoto describes the vibration as a mixture of vortex- and movement-induced vibration. He discovered a low-frequency shedding of enhanced vortices at inclined and yawed cables and an axial flow behind the cable (Matsumoto 2000). This high-speed vortex shedding might influence the excitation mechanism of rain-wind induced vibrations.

Most models are derived from the galloping theory. The vibrations are assumed to be movement induced. The position of the rivulet is given in advance and the aerodynamic forces are expressed as a function of the rivulet position and the cable velocity. The modified galloping theory as well as the empirical approach using energy considerations fail to describe the limited velocity range and the rivulet behaviour. Yamaguchi showed that only a model that accounts for both, the cable vibration and the movements of the rivulets, is capable of predicting the system behaviour adequately (Yamaguchi 1990). He modelled the vibrations similar to two-degree-of-freedom galloping using quasi-steady strip theory. In his model the movement of the rivulet is aerodynamically coupled to the cable vibration. The aerodynamic force acting on the cable are functions of the rivulet's position and the velocity of the cable and the rivulet.

The presented model now includes three degrees of freedom, all geometrical and physical nonlinearities of the coupled system, and also accounts for the frictional resistance between rivulet and cable surface. All forces caused by inertia, damping, stiffness, wind, friction, adhesion and inertial coupling are considered. The vibrations are assumed to be merely movement induced. Effects of additional excitation mechanisms like vortex shedding, gust or parametric excitation are omitted, but they might be relevant for the necessary initial disturbance of the system. Only one rivulet is considered.

2. Model

The system is modelled as a coupled two-mass oscillator with three degrees of freedom (Fig. 2). The cable can move translationally in cross-wind direction (y -direction) and in wind direction (z -direction) around its static equilibrium position. The cable has the diameter d and the mass m_s . It is supported by nonlinear springs and is viscously damped. Since large amplitudes are expected, the nonlinear behaviour of the cable is considered by the nonlinear spring stiffness (Tonis 1989). The rivulet moves tangentially on the cable surface, its position is given by the rotation angle φ . Its behaviour can be compared to a forced pendulum swinging around the moving center of the cable's cross section. The frictional resistance between rivulet and surface is simulated by a viscous damper. The angle β depends on the inclination angle δ of the cable and the wind direction given by the yaw angle γ .

$$\beta = \arctan\left(\frac{\sin \gamma \sin \delta}{\cos \gamma}\right) = \arctan(\tan \gamma \sin \delta) \quad (1)$$

The aerodynamic forces F_y , F_z and M_φ are assumed to be quasi-steady and independent of the Reynolds number. The following wind forces result from Fig. 3:

$$\begin{aligned} F_y &= -\frac{\rho}{2} \cdot d \cdot U_{rel}^2 \cdot [C_L(\alpha) \cos(\alpha_v) + C_D(\alpha) \sin(\alpha_v)] \\ F_z &= \frac{\rho}{2} \cdot d \cdot U_{rel}^2 \cdot [-C_L(\alpha) \sin(\alpha_v) + C_D(\alpha) \cos(\alpha_v)] \\ M &= \frac{\rho}{2} \cdot d^2 \cdot U_{rel}^2 \cdot C_M(\alpha) \end{aligned} \quad (2)$$

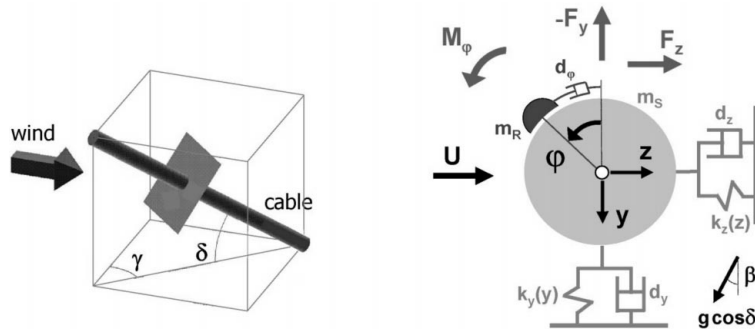


Fig. 2 Model

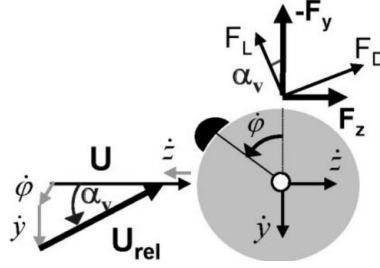


Fig. 3 Definitions

r is the distance between the centers of the two masses and ρ the air density. The aerodynamic coefficients C_L , C_D and C_M depend on the angle of attack and are approximated by polynomial functions.

The effective angle of attack α is a function of the momentary position of the rivulet and the velocities of the two masses (Fig. 3). The relative wind speed U_{rel} is assumed to be equal to the natural wind speed U , since the wind velocity is much higher than velocities of the two masses.

$$\alpha = -\varphi + \alpha_v = -\varphi + \tan\left(\frac{\dot{y} + r\dot{\varphi}\sin\varphi}{U - \dot{z} + r\dot{\varphi}\cos\varphi}\right) \cong -\varphi + \frac{\dot{y}}{U_{rel}} + \frac{r\dot{\varphi}\sin\varphi}{U_{rel}} \quad (3)$$

For the three degrees of freedom - the translations of the cable and the rotation of the rivulet - the equations of motion are calculated by Lagrangian functions. This results in three coupled differential equations of second order, where additional coupling terms and nonlinearities are included in the aerodynamic forces on the right-hand side. The first two equations describing the force equilibrium for the two translational degrees of freedom of the cable include the structural nonlinearities and coupling terms with the rivulet. The equivalence of the rivulet's behaviour to a pendulum is seen in the third equation. The first three terms are equal to the differential equation of a pendulum, the two following terms express the coupling with the cable movement. Calculations showed that the nonlinear response of the model is mainly caused by the nonlinearities and coupling terms of the aerodynamic forces on the right hand sides and the coupling between rivulet and cable seen in the third equation of Eq. (4). Nevertheless the structural nonlinearities are taken into account, because of the large amplitudes expected.

$$\begin{aligned} (m_S + m_R)\ddot{y} + d_y\dot{y} + k_y y + k_{y,2} y^2 + k_{y,3} y^3 + m_R r \sin\varphi \cdot \ddot{\varphi} + m_R r \cos\varphi \cdot \dot{\varphi}^2 &= F_y \\ (m_S + m_R)\ddot{z} + d_z\dot{z} + k_z z + k_{z,2} z^2 + k_{z,3} z^3 - m_R r \cos\varphi \cdot \ddot{\varphi} + m_R r \sin\varphi \cdot \dot{\varphi}^2 &= F_z \\ m_R r^2 \ddot{\varphi} + d_\varphi \dot{\varphi} - m_R r g \cos\delta \sin(\varphi + \beta) + m_R r \sin\varphi \cdot \ddot{y} - m_R r \cos\varphi \cdot \ddot{z} &= M_\varphi \end{aligned} \quad (4)$$

The system is analysed in phase space. Therefore, the differential equations are transformed into a system of equations of first order leading to a coupled system of six differential equations.

$$\dot{x} = f(x, \lambda) \quad x = (y, \varphi, z, \dot{y}, \dot{\varphi}, \dot{z})^T \quad (5)$$

$$\lambda = (U, d_y, m_R, \dots)$$

This coupled system of nonlinear equations is analysed by stability and bifurcation theory (Kuznetsov 1998).

3. Parameters

An example shall illustrate the features of the system. For the cable typical values for cables at cable-stayed bridges are chosen. The coefficients of the nonlinear terms are evaluated according to (Tonis 1989). The rivulet's parameters and the aerodynamic coefficients shown in Fig. 4 are taken from literature (Yamaguchi 1990, Verwiebe 1997, Gu & Lu 2001) or have been estimated based on first experimental results. Their values are currently determined more adequately by several experiments at the Institute for Steel Structures. The aerodynamic coefficients after Yamaguchi are taken as default values. As will be shown, even large variations in the parameters do not change the qualitative behaviour of the system.

Cable :	Rivulet :
diameter $d = 0.1$ m	height $h = 0.01$ m
mass $m_s = 50$ kg/m	mass $m_R = 0.2$ kg/m
frequency $f_y = f_z = 1$ Hz	damping $d_\varphi = 0.05$ Nms
damping $\xi_y = \xi_z = 2\%$ of crit.	Wind :
inclination $\delta = 45^\circ$	yaw angle $\gamma = 0^\circ$
$k_{y,3} = k_{z,3} = 0,00115$ N/m ³	angle $\beta = 0^\circ$
$k_{y,2} = 0,0077$ N/m ²	
$k_{z,2} = 0$ N/m ²	

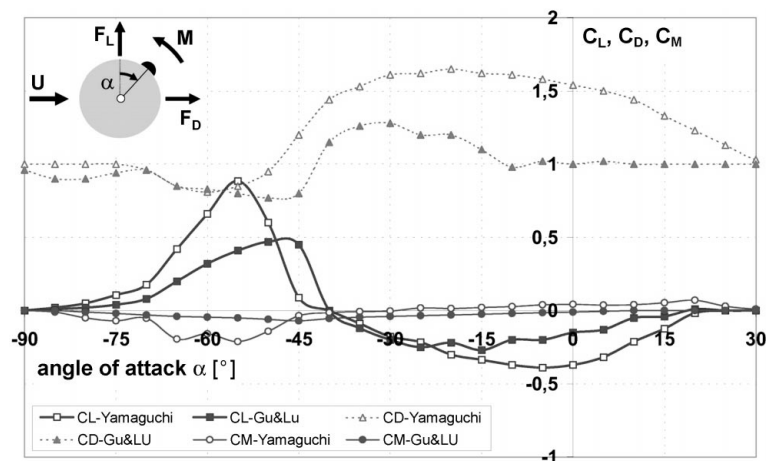


Fig. 4 Parameters and aerodynamic coefficients

The wind velocity is chosen as independent parameter while keeping the other parameters constant. The program CONTENT of Yu. A. Kuznetsov and V.V. Levitin was used for the numerical analysis of the given dynamical system.

4. Stability analysis

4.1. Stationary solutions / Static equilibrium positions

First the stationary points are calculated by

$$0=f(x_s, \lambda) \quad (6)$$

The system exhibits multiple solutions, as it is typical for nonlinear problems. Two and/or four static equilibrium positions are possible depending on the wind velocity. The stationary solutions for the rotational degree of freedom versus the wind velocity are shown in Fig. 5. For velocities less than 8 m/s two equilibria of the rivulet are possible: a lower position of equilibrium A (stable) and an upper position B (unstable). At a velocity of approximately 8 m/s a saddle-point bifurcation occurs. There are two more stationary solutions for velocities higher than 8 m/s (branches C and D).

4.2. Linear stability of the stationary solutions

Subsequently, the stability of these stationary points is determined by the linear stability theory according to Lyapunov. The eigenvalues of the Jacobian matrix J are evaluated.

$$\dot{x} = J(x_s, \lambda)x + O(x^2) + \dots \quad J = \left. \frac{\partial f}{\partial x} \right|_{x=x_s} \quad (7)$$

For a wind velocity less than 8 m/s, two stationary solutions exist. A stability analysis shows that solution A (lower position of rivulet) is always a stable focus. Solution B is an unstable saddle point.

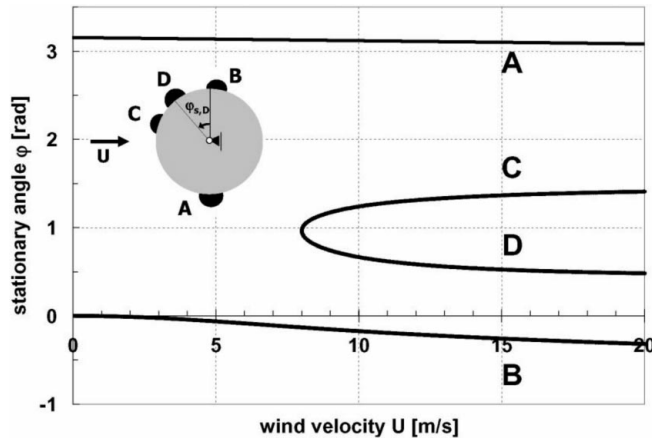


Fig. 5 Stationary points

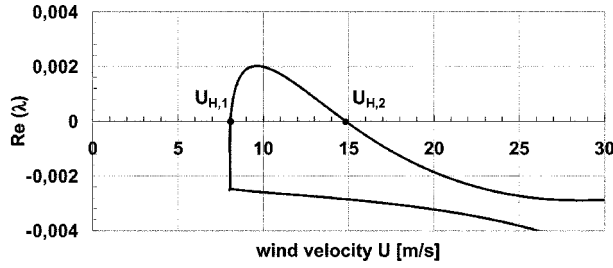


Fig. 6 Maximum realpart of eigenvalues

Like a pendulum, the rivulet always falls into the stable lower position *A*. For wind speeds of up to 8 m/s no excitation of the system occurs.

For velocities higher than 8 m/s two more stationary points exist. Stationary point *C* is an unstable saddle point like point *B*. Solution *D* is a focal point like solution *A*. Solutions *B* and *C* are unstable, the rivulet is driven away from these positions to a stable point of equilibrium. The only possible solution for a stable upper rivulet is then solution *D*. For velocities higher than 14.8 m/s, equilibrium *D* is stable (negative real part) as shown in Fig. 6. If the rivulet is initially formed between the unstable solutions *B* and *C*, the rivulet will move to the stable equilibrium position *D*. The branch *D* in Fig. 5 shows that an upper rivulet can form at an angle φ of 30°-60° depending on the wind velocity. The angle decreases with increasing wind speed as wind tunnel tests have demonstrated.

Below only the stability of solution *D* is examined. The maximum real part of the eigenvalues of solution *D* is shown as a function of wind speed in Fig. 6. Changes of stability, so-called Hopf bifurcations ($\text{Re}(\lambda)=0$), occur at U_{H1} and U_{H2} . In the region between these two velocities positive real parts exist, the solution is unstable. Thus, vibrations occur in this velocity range from 8–14.8 m/s.

4.3. Periodic solutions and nonlinear stability

The stationary solution between U_{H1} and U_{H2} is unstable. Now it is examined, if there are any periodic solutions with stable limit cycles in this velocity range. Therefore, also nonlinear terms in the differential equations have to be considered. Periodic solutions x_p are calculated by a shooting method evaluating the monodromy matrix M as a by-product (Seydel 1994). Periodic solutions with stable limit cycles exist, if the absolute value of the eigenvalues of the monodromy matrix, so-called characteristic multipliers, are smaller than and/or equal to 1.

$$\begin{aligned}
 M(x_p, \lambda) &= \Phi(T) & \dot{\Phi}(t) &= J(x_p, \lambda) \cdot \Phi(t) & x_p(t) &= x_p(t+T) \\
 & & \Phi(0) &= E & &
 \end{aligned} \tag{8}$$

where T is the period, E the identity matrix and Φ the fundamental solution matrix.

The nonlinear stability analysis yields one and/or three limit cycles depending on wind speed. One stable limit cycle exists in the ranges of $U = 8\text{-}10.7$ m/s and $12.7\text{-}14.8$ m/s. Between $10.7\text{-}12.7$ m/s three limit cycles exist, two are stable and one is unstable. In Fig. 7 the amplitude of the limit cycle vibrations are shown for the translational degrees of freedom. The amplitudes increase nonlinearly

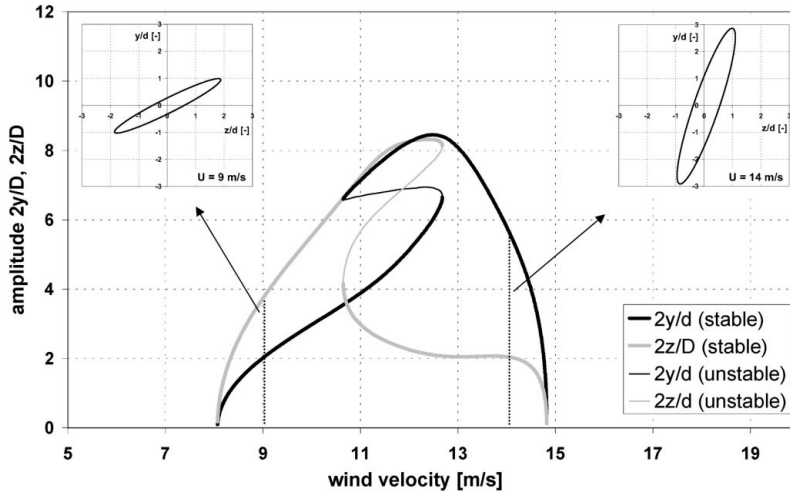


Fig. 7 Amplitude of the translational vibrations

with wind speed. In the ranges with one limit cycle the vibrations increase from a small initial disturbance until they reach the limit cycle amplitude. In the range from 8-10.7 m/s the system oscillates mainly in z -direction, whereas the vibration occurs in cross-wind direction for wind speeds of 12.7-14.8 m/s. These areas of soft excitation are separated by a region of possible hard excitation. Depending on the initial conditions (wind speed is increased or decreased), one of the two stable limit cycle oscillations occurs. Jump phenomena take place at the borders of this middle range. Thus, if the wind speed is constantly increased, the system starts to vibrate in mostly in-wind direction at 8 m/s. The direction of the oscillations changes abruptly at a wind speed of about 12.7 m/s. The system then vibrates mostly in cross-wind direction until 14.8 m/s is reached. The same phenomenon was observed in wind tunnel tests (Verwiebe 1997).

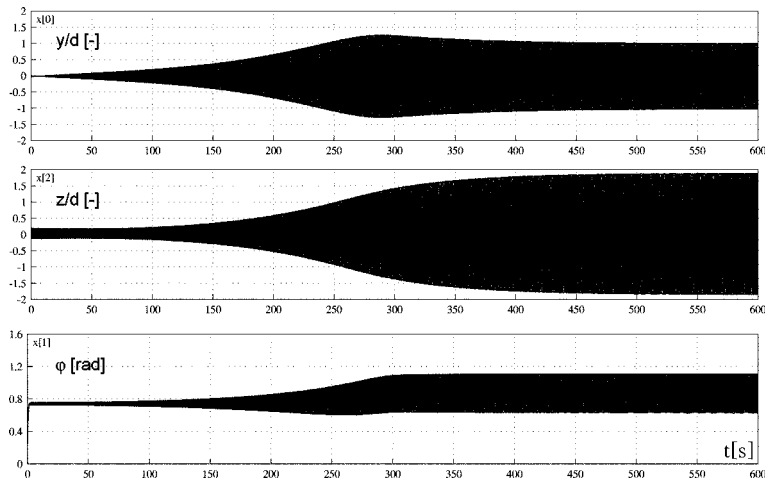


Fig. 8 Transient response at $U = 9$ m/s

The transient response of the cable translation and the rivulet rotation is shown in Fig. 8 for a wind speed of 9 m/s. Depending on the initial disturbance the time needed to reach the limit cycle oscillations exceeds more than 5 minutes. The rivulet rotates in its final state with an amplitude of approximately 25° about its stationary angle of about 45° .

5. Parametric study

The exact values of some parameters - especially the rivulet parameters like mass, shape and friction - are difficult to obtain and must be approximated. Some parameters are now varied to examine their effects on the system's behaviour. One parameter of particular interest is the damping of the cable. As observed in the field, increasing the cable damping, e.g. by external dampers, stops the rain-wind induced vibrations. Thus, the parameter effects are illustrated in stability diagrams plotting wind speed versus cable damping. For the stationary solution D , the stability diagram with all bifurcations is shown in Fig. 9. The saddle-point bifurcation of the stationary solution, Hopf bifurcations according to the linear stability theory, as well as the bifurcations according to the nonlinear theory are shown. The stability diagram is divided into three parts:

- region, where no stationary solution D exists
- stable region without excitation
- unstable region with periodic vibrations

For a degree of damping of 0.2%, the results of the sample calculation are obtained. If the wind speed is lower than 8 m/s, no stationary solution D exists, an upper rivulet cannot develop. This critical velocity is independent of cable damping (shaded region). At high wind speeds, an upper rivulet exists, but the system is stable. No excitation of vibrations occurs.

The unstable region, where periodic vibrations occur, is cross-hatched. As observed in situ and in experiments, the oscillations only occur in a limited range of wind speeds. The unstable velocity span decreases with increasing cable damping. For cable damping higher than a critical value ($\sim 0.7\%$) no excitation occurs any more. The model shows that rain-wind induced vibrations can be

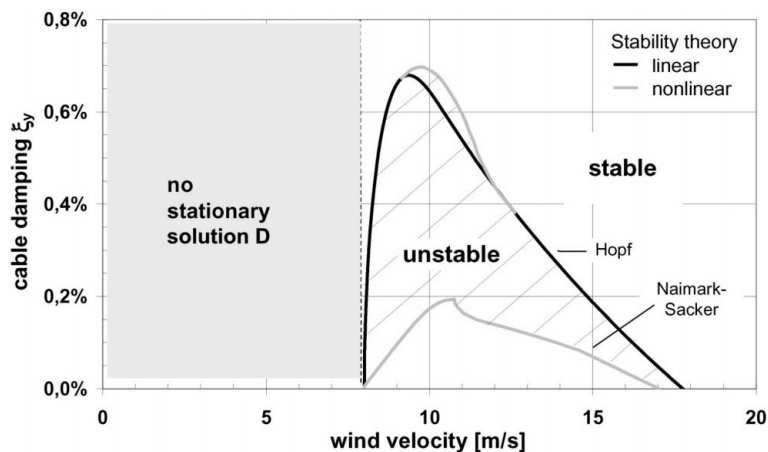


Fig. 9 Stability diagram

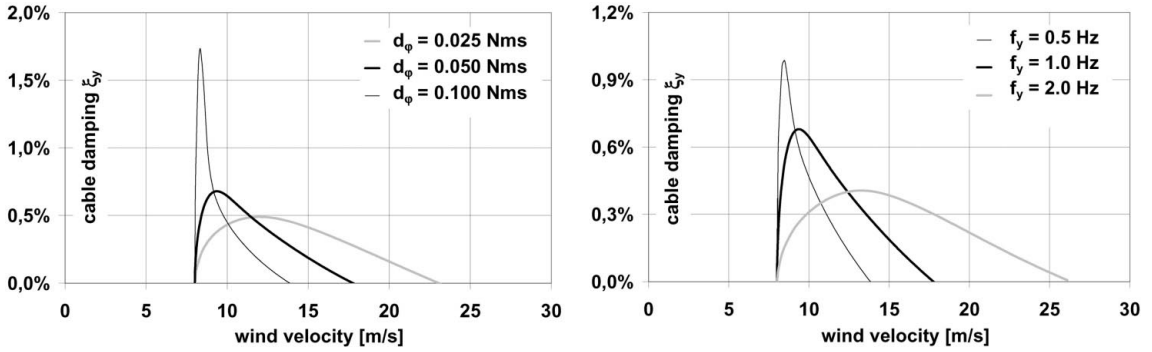


Fig. 10 Variation of rivulet damping and cable eigenfrequency

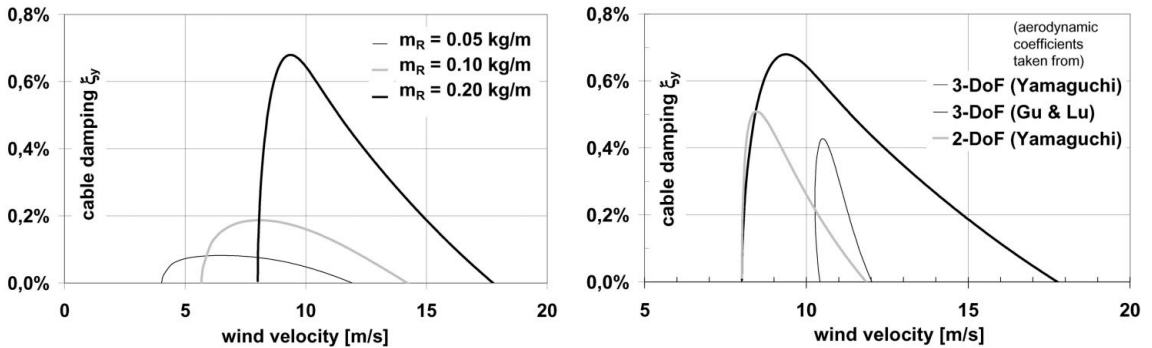


Fig. 11 Variation of rivulet mass, aerodynamic coefficients and DOF

stopped by increasing cable damping beyond that value, which is again in agreement with observations in situ. For low cable damping, bifurcations of higher order can take place. Quasi-periodic vibrations can occur after secondary Hopf bifurcations (Naimark-Sacker) or subharmonic vibrations after period doubling. Chaotic vibrations like the observed beat vibrations are possible after a sequence of these bifurcations at low cable damping.

Variations in different parameters are shown in Figs. 10 and 11. In these stability diagrams only the curves according to linear theory are plotted. The effect of the rivulet damping on the cable surface is illustrated in the first diagram of Fig. 10. For 3 different damping values the unstable regions are drawn showing that the qualitative behaviour of the system remains unchanged even at large variations. The onset velocity is the same for all three values. The unstable velocity region increases and the critical cable damping decreases with increasing rivulet damping. This influence of the rivulet damping might explain the dependence of the vibrations on the roughness/pollution of the cable surface observed in (Flamand 1994). The onset velocity is independent of the cable's eigenfrequency as shown in the second drawing.

The development of an upper rivulet formed by rain drops and the subsequent onset of vibrations can be explained by Fig. 11, where the influence of the rivulet mass is shown in the first diagram. Lighter rivulets have lower onset wind speed and smaller critical damping values meaning that lighter rivulets are stable at wind speeds, whereas heavy rivulets are unstable. Assuming the light

rivulet are rain drops on the cable surface, light rain drops that are initially between the unstable stationary points B and C are pushed into the stable position D (Fig. 5), forming a heavier upper rivulet. This rivulet leads then to the onset of cable vibrations.

Particularly crucial input parameters are the aerodynamic coefficients. Now the system stability is examined using aerodynamic coefficients from (Gu & Lu 2001) and compared with the former results obtained on the basis of the coefficients from Yamaguchi. The general profile of the aerodynamic coefficients is the same for both tests, even if the results from the two tests deviate in the aerodynamic coefficients of the momentum force on the rivulet (Fig. 4). Gu & Lu used smaller artificial rivulets ($h=6$ mm) than Yamaguchi, therefore the rivulet mass is now assumed to be 0.08 kg/m. To cause vibrations with the new coefficients required a yaw angle γ larger than 0° . A yaw angle of 45° was used here. Fig. 11 shows that even large deviations in the aerodynamic coefficients do not change the qualitative behaviour of the system. This fact can be explained by the same qualitative results from the two tests. In the specific range of angle of attack, where excitations occurs, all the aerodynamic coefficients exhibit steep slopes, especially in the lift force. This characteristic of the aerodynamic coefficients play the major part in the excitation mechanism.

In the second graph of Fig. 11 also the influence of the number of the degrees of freedom is shown. The authors showed in (Peil & Nahrath 2001) that already a model with two degrees of freedom, namely the cable translation in cross-wind direction and the rotation of the rivulet, is able to describe the phenomena of rain-wind induced vibrations. The more advanced model with an additional translational degree of freedom in wind direction exhibits a larger unstable region, but the same onset velocity.

6. Conclusions

The presented model - a coupled two-mass oscillator with three degrees of freedom - is able to simulate the phenomena of rain-wind induced vibrations. Both, the vibrations of the cable and the movement of the water rivulet on the cable surface can be described by the nonlinear model as well as the vibration's dependence on wind speed, cable damping and eigenfrequency. The results agree well with field data and wind tunnel tests. The model is robust, even large parameter variations do not change the qualitative behaviour of the system. The excitation mechanism of rain-wind induced vibration is closely linked to the coupled movements of the cable and the rivulet. The vibrations can be described as flutter of two coupled masses: the oscillator cable and the attached pendulum rivulet.

Several experiments are currently conducted to calibrate the input parameters of the model. The parameters of the rivulet, like its shape, mass, and friction on the cable surface, are determined as well as the aerodynamic coefficients for a cylinder with two rivulets. The model will be extended to simulate two rivulets.

Acknowledgements

The financial support of the Deutsche Forschungsgemeinschaft as part of the Graduate College "Interaction of Structure and Fluid" of the Technical University of Braunschweig is gratefully acknowledged.

References

- Bosdogianni, A. and Olivari, D. (1996), "Wind- and rain-induced oscillations of cables of stayed bridges", *J. Wind Eng. Ind. Aerod.*, **64**.
- Flamand, O. (1994), "Rain-wind induced vibration of cables", *Proc. of Int. Conf. on Cable-Stayed and Suspension Bridges* (AFPC), Deauville.
- Geurts, C.P.W. and van Staaldouin, P.C. (1999), "Estimation of the effects of rain-wind induced vibration in the design stage of inclined stay cables", *Proc. of the 10th ICWE*, Copenhagen.
- Gu, M. and Lu, Q. (2001), "Theoretical analysis of wind-rain induced vibration of cables of cable-stayed bridges", *Proc. of 5th APCWE*, Kyoto.
- Hikami, Y. and Shiraishi, N. (1988), "Rain-wind induced vibration of cables in cable-stayed bridges", *J. Wind Eng. Ind. Aerod.*, **29**.
- Kuznetsov, Yu. A. (1998), *Elements of Applied Bifurcation Theory*.
- Lüesse, G. et al. (1996), "Regen-Wind-induzierte Schwingungen an der Elbebrücke Dömitz", *Stahlbau*, **65** (German).
- Main, J.A. and Jones, N.P. (1999), "Full-scale measurements of stay cable vibration", *Proc. of the 10th ICWE*, Copenhagen.
- Matsumoto, M. (2000), "Aeroelasticity and bridge aerodynamics", *Proc. of Int. Advanced School on Wind-excited and Aeroelastic Vibrations of Structures*, Genova.
- Matsumoto, M., Daito, Y. et al. (1998), "Wind-induced vibration of cables of cable-stayed bridges", *J. Wind Eng. Ind. Aerod.*, **74-78**.
- Peil, U. and Nahrath, N. (2001), "Modellierung Regen-Wind induzierter Schwingungen", *WtG-Berichte Nr.7* (German).
- Ruscheweyh, H.P. (1999), "The mechanism of rain-wind-induced vibration", *Proc. of the 10th ICWE*, Copenhagen.
- Seydel, R. (1994), *Practical Bifurcation and Stability Analysis*, Springer.
- Tonis, D. (1989), "Zum dynamischen Verhalten von Abspannseilen", Dissertation Universität der Bundeswehr, München (German).
- Verwiebe, C. (1997), "Erregermechanismen von Regen-Wind induzierten Schwingungen", *WtG-Berichte Nr.5* (German).
- Yamaguchi, H. (1990), "Analytical study on growth mechanism of rain vibration of cables", *J. Wind Eng. Ind. Aerod.*, **3**.